ChemComm

COMMUNICATION

View Article Online
View Journal | View Issue

Cite this: *Chem. Commun.*, 2014, **50**, 6740

Received 17th February 2014,
Accepted 28th April 2014

DOI: 10.1039/c4cc01251h

www.rsc.org/chemcomm

Mn^{II}-containing coordination nanoparticles as highly efficient T_1 contrast agents for magnetic resonance imaging†

Gabriella Paul,[a] Yoann Prado,[a] Nada Dia,[ab] Eric Rivière,[a] Sophie Laurent,[c] Mathieu Roch,[d] Luce Vander Elst,[cd] Robert N. Muller,[cd] Lucie Sancey,[e] Pascal Perriat,[f] Olivier Tillement,[e] Talal Mallah[a] and Laure Catala*[a]

Large longitudinal relaxivities were observed in Mn^{II}-containing Prussian blue analogue nanoparticles. At low concentrations and high field (7 T), a remarkable positive contrast enhancement was seen which exceeded that of clinical contrast agents and was attributed to the very large proportion of surface atoms of these coordination nanoparticles.

Magnetic resonance imaging (MRI) is a non-invasive technique that allows the diagnosis of diseased zones. In 30% of clinical tests, contrast agents (CAs) are used to enhance the image quality. Designing positive CAs denoted as T_1-CAs with larger longitudinal relaxivities (r_1) is one way to reduce the injected dose into the patient. The brightening conferred by such CAs originates from the fast proton relaxation of water molecules coordinated to paramagnetic ions with a large spin, a long electronic relaxation time and a fast water exchange rate such as in Gd^{III} chelates commonly used as clinical CAs and in Mn^{II} complexes.[1–3] One valuable strategy to improve their efficiency and delay their blood clearance is to use larger structures including these paramagnetic complexes or ions. A longer rotational correlation time leading to an enhanced longitudinal relaxivity is the result of slow tumbling due to the high molecular weight of the nano-object.[1,2] This has been reported for Gd^{III} and Mn^{II} complexes grafted on polymers, particles, proteins and in liposomes.[1–11] Nevertheless, in general local reorientation of the complexes leads to low values of relaxivities. Hence, active paramagnetic species directly included into the core of NPs is a way to circumvent this problem, as described for some Gd^{III} and Mn^{II} oxides,[7,8,12–17] fluorides[18] and metal organic frameworks.[19–25] Among microporous networks, cyano-bridged coordination networks such as Prussian blue analogue (PBA) NPs have been extensively investigated for their magnetic/electronic properties,[26–29] but less focus has been placed on MRI-CAs, despite the FDA approval of Prussian blue. Citrate coated Prussian blue NPs of 13 nm have been reported[30,31] with a modest negative (T_2) contrast enhancement, while Gd^{III}-containing polycyanometallate NPs below 5 nm coated with polysaccharides (either in acidic[32] or neutral[33,34] aqueous media) and PB NPs containing Gd^{III}[35] structures of around 100 nm revealed high longitudinal relaxivities. Recently, large Mn^{II} PBA particles have been reported (on exchange resin or with silica) with large transverse relaxivities ($100 < r_2 < 205$ mM^{-1} s^{-1}) that are adapted to T_2-weighted images.[36]

In this communication, $K_{4y-3+x}Mn^{II}{}_xIn^{III}{}_{1-x}$ $[Fe^{II}(CN)_6]_y$ NPs with controlled contents of Mn^{II} have been obtained between 5 and 21 nm through coprecipitation by a one-step process in water without any additional reactant, followed by post-coating by dextran. These new compounds (abbreviated as MnInFe@Dextran NPs) exhibit large longitudinal relaxivities for Mn^{II}-based CAs (and r_2/r_1 close to 2) that exceed those of Mn^{II} oxide NPs. A remarkable positive T_1 contrast enhancement was registered exceeding that of clinical chelate Gd-DTPA (Magnevist) under conditions usually unfavorable to T_1 paramagnetic oxide NPs, *i.e.* at a low paramagnetic ion concentration (0.2 mM of Mn^{II}) under high field (7 T) and with short TR MRI sequences.

Nanoparticles were produced without any additive by fast mixing of an aqueous solution of hexacyanoferrate(II) with an aqueous solution containing Mn^{II} and In^{III} salts in variable ratios, $x = [Mn^{II}]/[In^{III}]$ from $x = 0.05$ to $x = 0.9$ (see ESI†).

Formation of stable colloidal solutions without aggregation was monitored by dynamic light scattering (DLS) and the results reveal hydrodynamic diameters that depend on the Mn^{II} ions content for $x > 0.4$ (Fig. S1, ESI†). Without the introduction

[a] *Institut de Chimie Moléculaire et des Matériaux d'Orsay, CNRS, Université Paris 11, 91405 Orsay, France. E-mail: laure.catala@u-psud.fr; Fax: +33169154754; Tel: +33169157890*
[b] *Ecole Doctorale des Sciences et de Technologie, Hadath campus P.O. Box 5, Université Libanaise Beyrouth, Lebanon*
[c] *Univ Mons, NMR & Mol Imaging Lab, Dept Gen Organ & Biomed Chem, B-7000 Mons, Belgium*
[d] *CMMI: Center for Microscopy and Molecular Imaging, Rue Adrienne Bolland, 8, B-6041 Gosselies, Belgium*
[e] *Institut Lumière Matière Equipe FENNEC - UMR CNRS 5306 - Univ. Lyon 1Bâtiment Jules Raulin, 2, rue V. Grignard, 69622 Villeurbanne, France*
[f] *INSA Lyon, 7, Avenue Jean Capelle, 69621 Villeurbanne, France*

† Electronic supplementary information (ESI) available: Synthetic procedures and detailed XRD, DLS, IR, and elemental analysis TEM data. See DOI: 10.1039/c4cc01251h

of In^{III} ions ($x = 1$), the colloidal solution was unstable. Introduction of only 10% of In^{III} ions enables the control of NPs with hydrodynamic diameters below 20 nm while 90% of In^{III} ions lead to a hydrodynamic diameter of 7 nm. This is related to the high insolubility of InFe PBA that controls the nucleation rate. Powders of NPs obtained with $0.05 < x < 0.9$ were recovered by adding 25 equivalents of the dextran monomer per ferrocyanide and flocculation with acetone. MnInFe@Dextran NPs were subsequently dispersed in water up to 10 mM with stability for over a period of months without any change in the hydrodynamic diameter. Transmission electron microscopy (TEM) was carried out on these dispersions which revealed homogeneous nanoparticles isolated by dextran chains, with an average size ranging from 4 ± 1 nm to 20.7 ± 3.5 nm for $x = 0.05$ and $x = 0.9$, respectively (Fig. 1 inset and Fig. S2, ESI†). X-ray powder diffraction performed on the powders confirmed the face centered cubic structure of the NPs in all samples (Fig. S3, ESI†), with a decrease of the average cell parameter from 10.43 Å to 10.13 Å as the Mn^{II} ion content increased from $x = 0.05$ to $x = 0.9$, which is in good agreement with the smaller ionic radius of the Mn^{II} ion compared to that of the In^{III} ion. This indicates that Mn^{II} ions are not inserted in the coordination network. Fourier transform infra-red (FT-IR) spectra recorded for the different compounds revealed a broad band with two contributions at 2067 cm^{-1} and 2108 cm^{-1} that were attributed to the superimposed asymmetric vibrations of the bridged cyanides Mn^{II}–NC–Fe^{II} and In^{III}–NC–Fe^{II}, respectively, with the most intense contributions shifted to low frequencies for larger Mn^{II} proportions (Fig. S4, ESI†). The composition of metal ions and dextran was assessed by elemental analysis (Fig. S5, ESI†) that showed a decrease of the ferrocyanide vacancies from 20% to 10% upon decreasing x. It is possible to estimate the number of dextran chains (~100) from the size and composition considering an average degree of polymerization of 247, leading to around 3 anchoring points between each chain and the surface of NPs. Magnetic measurements recorded at 5 K (Fig. S6, ESI†) confirmed the paramagnetic behaviour of all samples, with a coherent increase of the magnetization value at 5 T as the Mn^{II} contents were increased (the other ions In^{III} and low spin Fe^{II} are diamagnetic). Relaxometry measurements were registered at 37 °C (310 K) under a field of 1.5 T on the colloidal solutions obtained for samples with $0.05 < x < 0.9$ (Fig. 1).

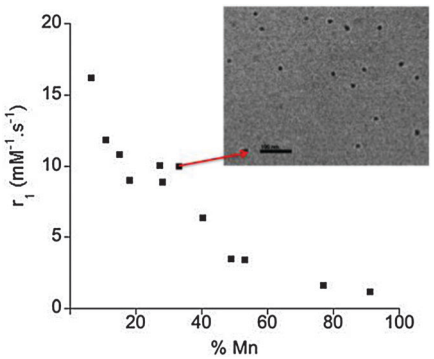

Fig. 1 Longitudinal relaxivity r_1 dependence of MnInFe@Dextran NPs on different Mn^{II} ion contents. Inset: the TEM image of NP-33%.

The longitudinal and transverse relaxivities r_i (i = 1 and 2 respectively) expressed per mM of Mn^{II} ions (the other ions being diamagnetic) show a strong dependence on the Mn^{II} content indicating that all Mn^{II} ions are not equivalent depending on their location at the surface or in the core of the particles. Large longitudinal relaxivities between r_1 = 9 mM^{-1} s^{-1} up to r_1 = 15 mM^{-1} s^{-1} have been determined for samples with $x = 0.3$ to $x = 0.05$, respectively. A value of r_1 = 15 mM^{-1} s^{-1} per Mn^{II} ion is 40 times that of 7 nm MnO nanoparticles[15] and about twice that reported for the best 2.5 nm MnO nanoparticles[7,8] (also recorded at 1.5 T). Since in this range of the Mn^{II} content the size of particles is around 5 nm, the high proportion of Mn^{II} ions located at the surface of particles (calculated to be around 45%, Fig. S7, ESI†) may explain this efficiency, as these ions have a larger number of coordinated water molecules during efficient exchange with bulk water.‡ Upon increasing the Mn^{II} proportion from $x = 0.4$ to $x = 0.9$, the r_1 values decreased from 5 mM^{-1} s^{-1} to 1.6 mM^{-1} s^{-1} (expressed per mM of Mn^{II} ions). In this range of the Mn^{II} content, the size of particles increases together with the Mn^{II} content resulting in (i) a decrease of the relative quantity of ions located at the surface of nanoparticles and (ii) an increase in the number of Mn^{II} ions located in the core of the particles and thus less activity upon proton relaxation. The transverse relaxivities r_2 follow the same trend as that followed by r_1 with values comprised between 30 mM^{-1} s^{-1} and 1.4 mM^{-1} s^{-1} (per mM of Mn^{II} ions), and r_2/r_1 ratios between 1.1 and 1.8, which confirm that these particles are expected to behave as positive CAs (Fig. S8, ESI†). These measurements were reproduced for different batches of particles.

Among the various samples, nanoparticles with a proportion of 33% Mn ($x = 0.33$ denoted as NP-33%) were selected as they display the best relaxivity for the minimum total amount of metallic ions of Fe^{II}, In^{III} and Mn^{II} (see calculation in Fig. S9, ESI†). The nuclear magnetic relaxation dispersion (NMRD) profile of NP-33% at 37 °C shows a typical frequency dependence of r_1 for slow tumbling CAs, which confirms that Mn^{II} ions are incorporated in the core of NPs (Fig. 2a). In addition, the low frequency profile discards any free Mn^{II} ions. The decrease of longitudinal relaxivity r_1 at 300 MHz (7 T) is similar to that usually observed

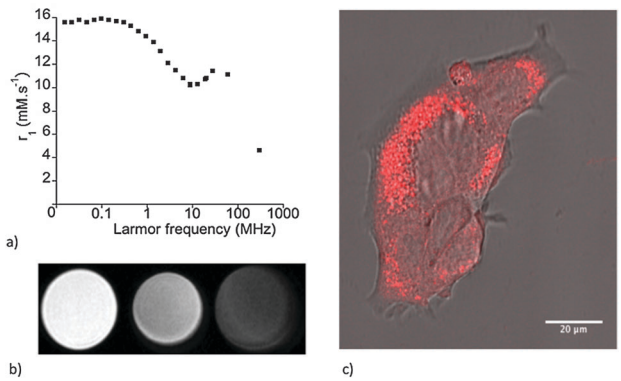

Fig. 2 (a) NMRD profile of NP-33% at 37 °C (b) T_1-weighted MR images of left: NP-33% at [Mn^{II}] = 0.2 mM, center: Gd-DTPA clinical CA at [Gd^{III}] = 0.2 mM and right: water, from a 7 T clinical MRI system with a spin gradient sequence with TR = 22 ms and TE = 3 ms. (c) Cell internalization of NP-33% coated by Dextran-TRITC after 60 min.

for paramagnetic nanoparticles. Longitudinal relaxivity was also registered at 60 MHz (3 T) at 5 °C which increases from r_1 = 10.0 mM^{-1} s^{-1} at 37 °C to 12.9 mM^{-1} s^{-1} at 5 °C (Fig. S10, ESI†), suggesting that the water exchange is not the limiting parameter but rather the rotational correlation time is. In addition, the filtrate obtained after ultrafiltration of the colloidal solution was analyzed: its relaxation time is similar to that of water, and ICP measurement reveals negligible Mn^{II} and In^{III} contents (4 μg L^{-1} for Mn^{II}, *i.e.* 75 nM corresponding to 0.4% of the initial concentration and below the detection threshold for In^{III}, *i.e.* less than 2% of the initial concentration), which confirm the high stability of these nano-objects. This is further supported by a constant value of the longitudinal relaxation time T_1 recorded on the stable colloidal solution after 6 months and by DLS measurements recorded in serum at 5 mM (Fig. S11, ESI†).

Importantly, a large T_1-weighted contrast enhancement was observed for NP-33% under a field of 7 T (300 MHz) at a concentration of 0.2 mM in Mn^{II} ions exceeding that of Gd-DTPA (Fig. 2b). The high contrast observed at high field and low concentrations may be further increased if recorded at 3 T (60 MHz). This highlights the remarkable activity of NP-33% as a T_1-CA compared to Mn^{II}-based oxides (that are usually compared to pure water). This efficiency can be related to a moderate r_2 (and thus low r_2/r_1) due to a weak number of paramagnetic sites contained in these 5 nm NPs (only 240 Mn^{II} atoms per particle, since In^{III} and Fe^{II} are diamagnetic) combined to the efficient exchange of water on the Mn^{II} atoms located at the periphery of NPs. Indeed, the presence of dextran does not impede the exchange of water molecules as the "bare" NP-33% have a smaller relaxivity (r_1 = 7 mM^{-1} s^{-1} at 37 °C and 1.5 T) compared to coated NP-33%, due to the decrease of the rotational correlation time. This again suggests that the former is the parameter limiting the relaxivity of these nanosystems.

Cytotoxicity of NP-33% was examined by the MTT test performed on two cell lines. The HEK293 cells were unaffected after 24 h below 5 mM concentrations of NP-33% and comparable to pure dextran (no toxicity at 8 mg mL^{-1}, Fig. S12, ESI†). Murin mammalian cells revealed an IC_{50} of 3.8 mg mL^{-1} (532 μM of NP-33%) after 24 h, while it remained non-toxic for short times (1 h) up to 19 mg mL^{-1} (2 mM, Fig. S12, ESI†). In summary, NP-33% were observed to be non-toxic to weakly toxic up to fairly high concentrations for short and long times, respectively, and appears to be dependent on the cell line. *In vitro* studies were also performed to monitor cell internalization by confocal microscopy at λ = 500–700 nm using NP-33% coated with dextran chains labeled with 0.1% of the fluorescent tetramethylrhodamine (TRITC) (Fig. S13, ESI†) and were fully characterized as the unlabelled ones (Fig. S14, ESI†). Fast internalization in less than 30 min was observed with the formation of vesicles (Fig. 2c and Fig. S15, ESI†) and no penetration was detected in the cell nucleus.

In summary, the high proportion of atoms located at the surface of these nanoparticles as compared to oxide or metal nanoparticles due to the low metallic density of microporous PBAs leads to remarkable longitudinal relaxivities per Mn^{II} atom among the largest reported for Mn^{II} with along that of Si quantum dot clusters doped with Mn^{II}.[37] As a consequence of a low r_2/r_1 ratio, a large T_1-contrast enhancement is registered at low concentrations of Mn^{II} ions under high field conditions and short MRI sequences exceeding that of Gd-based clinical CAs. Their high stability, low toxicity and water-based preparation at room temperature make this family of Mn^{II}-based PBA contrast agents promising candidates for *in vivo* MRI diagnosis. Incorporation of ^{111}In and other active probes for single photon emission computed tomography (SPECT) will lead to multimodality on these new CAs.[38]

Authors thank the Center for Microscopy and Molecular Imaging (CMMI, supported by the European Regional Development Fund and the Walloon Region). This work was supported by the Walloon Region (program First spin-off), FNRS (Fond National de la Recherche Scientifique), UIAP VII and ARC Programs of the french Community of Belgium, BELSPO, COST Actions (D38 and TD1004), the EMIL program, the French CNRS, the Université Paris Sud, the Institut Universitaire de France, the Lebanese CNRS and the Université Libanaise for their financial support. We thank Philippe Mejanelle for ICP measurements.

Notes and references

‡ Because of less than 10% ferrocyanide vacancies in this range of the Mn^{II} content and albeit the microporosity of the network, internal Mn^{II} ions that bear a small number of water molecules are not expected to play a relevant role in these compounds.

1 P. Caravan, J. J. Ellison, T. J. McMurry and R. B. Lauffer, *Chem. Rev.*, 1999, **99**, 2293–2352.
2 R. B. Lauffer, *Chem. Rev.*, 1987, **87**, 901–927.
3 B. Drahos, I. Lukes and E. Toth, *Eur. J. Inorg. Chem.*, 2012, 1975–1986.
4 S. Laurent, C. Henoumont, L. Vander Elst and R. N. Muller, *Eur. J. Inorg. Chem.*, 2012, 1889–1915.
5 S. Aime, D. D. Castelli, D. Lawson and E. Terreno, *J. Am. Chem. Soc.*, 2007, **129**, 2430–2431.
6 E. Tóth, R. D. Bolskar, A. Borel, G. Gonzalez, L. Helm, A. E. Merbach, B. Sitharaman and L. J. Wilson, *J. Am. Chem. Soc.*, 2005, **127**, 799–805.
7 M. Kueny-Stotz, A. Garofalo and D. Felder-Flesch, *Eur. J. Inorg. Chem.*, 2012, 1987–2005.
8 Z. P. Zhen and J. Xie, *Theranostics*, 2012, **2**, 45–54.
9 C. Alric, J. Taleb, G. Le Duc, C. Mandon, C. Billotey, A. Le Meur-Herland, T. Brochard, F. Vocanson, M. Janier, P. Perriat, S. Roux and O. Tillement, *J. Am. Chem. Soc.*, 2008, **130**, 5908–5915.
10 L. Moriggi, C. Cannizzo, E. Dumas, C. R. Mayer, A. Ulianov and L. Helm, *J. Am. Chem. Soc.*, 2009, **131**, 10828–10829.
11 M. F. Ferreira, B. Mousavi, P. M. Ferreira, C. I. O. Martins, L. Helm, J. A. Martins and C. F. G. C. Geraldes, *Dalton Trans.*, 2012, **41**, 5472–5475.
12 J. L. Bridot, A. C. Faure, S. Laurent, C. Rivière, C. Billotey, B. Hiba, M. Janier, V. Josserand, J. L. Coll, L. Vander Elst, R. Muller, S. Roux, P. Perriat and O. Tillement, *J. Am. Chem. Soc.*, 2007, **129**, 5076–5084.
13 T. Kim, E. Momin, J. Choi, K. Yuan, H. Zaidi, J. Kim, M. Park, N. Lee, M. T. McMahon, A. Quinones-Hinojosa, J. W. M. Bulte, T. Hyeon and A. A. Gilad, *J. Am. Chem. Soc.*, 2011, **133**, 2955–2961.
14 H. B. Na and T. Hyeon, *J. Mater. Chem.*, 2009, **19**, 6267–6273.
15 H. B. Na, J. H. Lee, K. J. An, Y. I. Park, M. Park, I. S. Lee, D. H. Nam, S. T. Kim, S. H. Kim, S. W. Kim, K. H. Lim, K. S. Kim, S. O. Kim and T. Hyeon, *Angew. Chem., Int. Ed.*, 2007, **46**, 5397–5401.
16 T. Yu, J. Moon, J. Park, Y. I. Park, H. Bin Na, B. H. Kim, I. C. Song, W. K. Moon and T. Hyeon, *Chem. Mater.*, 2009, **21**, 2272–2279.
17 M. I. Shukoor, F. Natalio, M. N. Tahir, M. Wiens, M. Tarantola, H. A. Therese, M. Barz, S. Weber, M. Terekhov, H. C. Schroder, W. E. G. Muller, A. Janshoff, P. Theato, R. Zentel, L. M. Schreiber and W. Tremel, *Adv. Funct. Mater.*, 2009, **19**, 3717–3725.
18 N. J. J. Johnson, W. Oakden, G. J. Stanisz, R. S. Prosser and F. C. J. M. van Veggel, *Chem. Mater.*, 2011, **23**, 4877.
19 W. J. Rieter, K. M. L. Taylor, H. Y. An, W. L. Lin and W. B. Lin, *J. Am. Chem. Soc.*, 2006, **128**, 9024–9025.

20 K. M. L. Taylor, W. J. Rieter and W. B. Lin, *J. Am. Chem. Soc.*, 2008, **130**, 14358–14359.
21 K. M. L. Taylor-Pashow, J. Della Rocca, Z. G. Xie, S. Tran and W. B. Lin, *J. Am. Chem. Soc.*, 2009, **131**, 14261.
22 P. Horcajada, T. Chalati, C. Serre, B. Gillet, C. Sebrie, T. Baati, J. F. Eubank, D. Heurtaux, P. Clayette, C. Kreuz, J. S. Chang, Y. K. Hwang, V. Marsaud, P. N. Bories, L. Cynober, S. Gil, G. Ferey, P. Couvreur and R. Gref, *Nat. Mater.*, 2010, **9**, 172–178.
23 P. Horcajada, R. Gref, T. Baati, P. K. Allan, G. Maurin, P. Couvreur, G. Ferey, R. E. Morris and C. Serre, *Chem. Rev.*, 2012, **112**, 1232–1268.
24 D. Cunha, M. Ben Yahia, S. Hall, S. R. Miller, H. Chevreau, E. Elkaim, G. Maurin, P. Horcajada and C. Serre, *Chem. Mater.*, 2013, **25**, 2767–2776.
25 A. Carne-Sanchez, C. S. Bonnet, I. Imaz, J. Lorenzo, E. Tóth and D. Maspoch, *J. Am. Chem. Soc.*, 2013, **135**, 17711–17714.
26 L. Catala, F. Volatron, D. Brinzei and T. Mallah, *Inorg. Chem.*, 2009, **48**, 3360–3370.
27 L. Catala, A. Gloter, O. Stephan, G. Rogez and T. Mallah, *Chem. Commun.*, 2006, 1018–1020.
28 N. Galvez, P. Sanchez and J. M. Dominguez-Vera, *Dalton Trans.*, 2005, 2492–2494.
29 J. Larionova, Y. Guari, C. Sangregorio and C. Guerina, *New J. Chem.*, 2009, **33**, 1177–1190.
30 M. Shokouhimehr, E. S. Soehnlen, J. H. Hao, M. Griswold, C. Flask, X. D. Fan, J. P. Basilion, S. Basu and S. P. D. Huang, *J. Mater. Chem.*, 2010, **20**, 5251–5259.
31 M. Shokouhimehr, E. S. Soehnlen, A. Khitrin, S. Basu and S. P. D. Huang, *Inorg. Chem. Commun.*, 2010, **13**, 58–61.
32 Y. Guari, J. Larionova, M. Corti, A. Lascialfari, M. Marinone, G. Poletti, K. Molvinger and C. Guerin, *Dalton Trans.*, 2008, 3658–3660.
33 E. Chelebaeva, J. Larionova, Y. Guari, R. A. S. Ferreira, L. D. Carlos, A. A. Trifonov, T. Kalaivani, A. Lascialfari, C. Guerin, K. Molvinger, L. Datas, M. Maynadier, M. Gary-Bobo and M. Garcia, *Nanoscale*, 2011, **3**, 1200–1210.
34 M. Perrier, S. Kenouche, J. Long, K. Thangavel, J. Larionova, C. Goze-Bac, A. Lascialfari, M. Mariani, N. Baril, C. Guerin, B. Donnadieu, A. Trifonov and Y. Guari, *Inorg. Chem.*, 2013, **52**, 13402–13414.
35 M. F. Dumont, H. A. Hoffman, P. R. Yoon, L. S. Conklin, S. R. Saha, J. P. Paglione, R. W. Sze and R. Fernandes, *Bioconjugate Chem.*, 2014, **25**, 129–137.
36 S. D. Huang, Y. Li and M. Shokouhimehr, WO 2011/106309 A2, 2011; S. D. Huang, A. K. Khitrin and V. S. Perera, WO 2012/108856 A1, 2012.
37 C. Q. Tu, X. C. Ma, P. Pantazis, S. M. Kauzlarich and A. Y. Louie, *J. Am. Chem. Soc.*, 2010, **132**, 2016–2023.
38 T. J. Wadas, E. H. Wong, G. R. Weisman and C. J. Anderson, *Chem. Rev.*, 2010, **110**, 2858–2902.